Hindawi
Geofluids
Volume 2022, Article ID 8424055, 14 pages
https://doi.org/10.1155/2022/8424055

Research Article

Study on the Response of Staggered Floor Isolated Structures in Mountainous Areas under Three-Dimensional Earthquakes

Shishan Cheng,[1] **Jie Yang**,[2] **Dewen Liu**,[1] **Lihao Chen**,[1] **Feng Wan**,[1] **Fan Yang**,[1] **and Yang Liu**[3]

[1]*College of Civil Engineering, Southwest Forestry University, Kunming 650000, China*
[2]*College of Engineering and Technology, The Open University of Sichuan, Chengdu 610031, China*
[3]*College of Civil Engineering, Tongji University, Shanghai 200092, China*

Correspondence should be addressed to Dewen Liu; civil_liudewen@sina.com

Received 5 February 2022; Revised 17 May 2022; Accepted 13 June 2022; Published 12 July 2022

Academic Editor: Yue Niu

As coal mines are susceptible to safety accidents due to earthquakes, the requirements for structures in coal mining areas such as fire control centers and hospitals are higher, so base isolated structures, including staggered isolated structures, adapted to mountainous terrain are used in mining areas. The staggered floor isolated structure is a kind of isolated structure in mountainous areas which developed from the base-isolated structure. The theoretical research on staggered isolated structures is relatively few, and the theoretical research lags behind the practical application of engineering. In this paper, three staggered floor isolated structures with different heights of staggered floors are established. The responses of structures under one-dimensional, two-dimensional, and three-dimensional earthquakes are analyzed by the finite element dynamic time-history analysis method. The structural torsion, interstory shear force, maximum axial force, and floor displacement of the structure are compared. Due to the asymmetric characteristics of the staggered floor isolated structure, the center of stiffness of the staggered floor isolated structure deviates from the center of mass, which produces not only horizontal vibration but also obvious torsional vibration. The input of earthquakes in different dimensions also makes a difference in the response of the structure. The location between the upper isolated layer and the first floor above the upper isolated layer is a weak point of the structure. The results obtained in this study are distinguished from traditional basic isolated structures, which supplements the theoretical research of the staggered isolated structure.

1. Introduction

As coal mines are susceptible to safety accidents due to earthquakes, the requirements for structures in coal mine areas such as fire control centers and hospitals are higher; the function of these structures should be ensured under earthquakes. So base isolated structures, including staggered isolated structures, adapted to mountainous terrain are used in mining areas. In the base isolated research, the isolated layer is located at the same level, and horizontal movement of the whole building occurred mainly at the isolated layer when an earthquake occurs, which reduces the response of the structure. The theoretical research and practical application of horizontal seismic action are more mature. For example, Cheng et al. [1] used the finite element software ABAQUS to build a high-rise isolated structure to simulate earthquakes induced by hydraulic fracturing. Then, the nonlinear dynamic response of the structure considering the SSI (soil-structure interaction) effect was analyzed. It was found that the base shear force and interlayer displacement of the isolated structure without considering SSI were significantly larger than those with SSI. The base shear displacement was larger than that of soft soil layers when using hard soil layers. Chen et al. [2] used a one-dimensional equivalent linear method to numerically analyze vibration effects of the ground in loess areas. The results show that the response of typical loess areas under different seismic excitations has completely different dynamic characteristics; the damage of the earthquake in loess areas under far-field seismic excitation

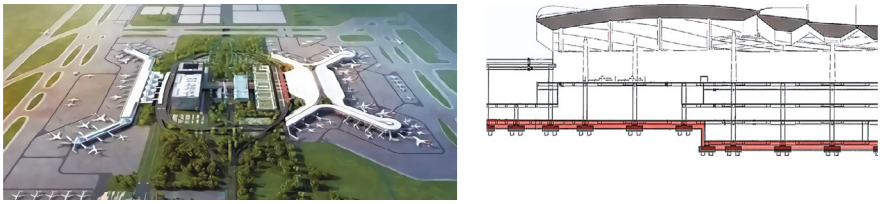

(a) Panoramic rendering of the project (b) Partial elevation of staggered floor isolated

Figure 1: Haikou Meilan Airport.

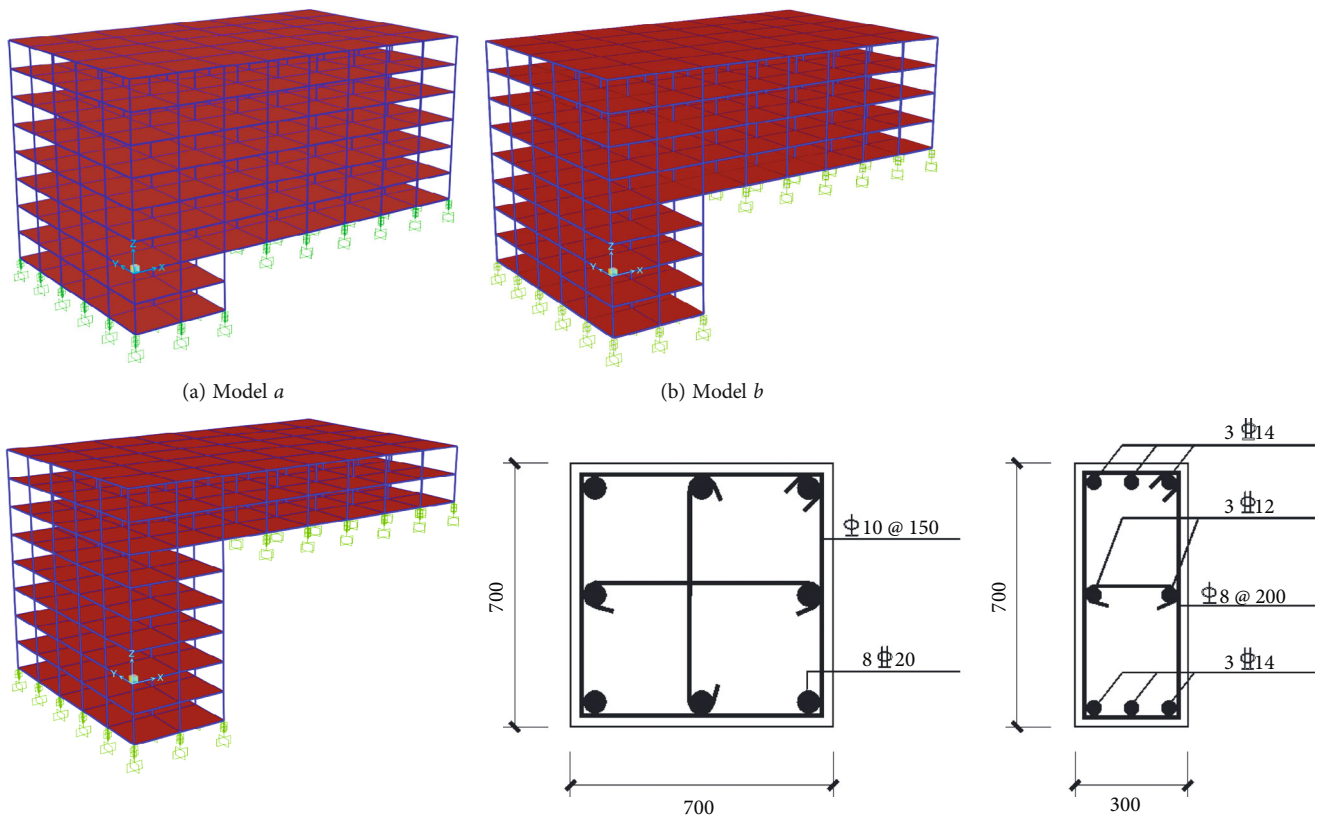

(a) Model *a* (b) Model *b*

(c) Model *c* (d) Columns and beams

Figure 2: Structural model and reinforcement schematic.

is more severe than that under near-field seismic excitation at the same peak acceleration. Nie et al. [3] studied the seismic compression ratios of sandy soils subjected to two mutually perpendicular horizontal components of the earthquake, as well as the seismic compression ratio of sandy soils with a single horizontal component of the earthquake. The results show that the ratio generally ranges from 1.52 to 2.32, which increases with the magnitude and the relative density of the sandy soil and decreases with the increase in the epicenter distance. Hashemi and Aghashiri [4] used an equivalent mechanical model of a rectangular vessel with three concentrated masses and six degrees of freedom. The results show that base isolation can effectively reduce responses such as base shear, wall deflection, and dynamic water pressure but can adversely affect the free surface sway height. The people's hospital in Lushan County, which adopted the isolated technology, remained intact after the 2010 Ya'an earthquake [5].

In the research on three-dimensional earthquakes, a large number of disaster records show that the decisive damage to buildings is not entirely the horizontal component of the earthquake, so it is necessary to consider the vertical component of the earthquake. For example, the vertical component amplitude recorded by the IWTH25 station was as high as 4000 gals in the 2008 Nairiku earthquake in Miyagi Prefecture, Japan [6]. The high vertical acceleration peaks were also measured in the aftershocks of the Tangshan earthquake, and some even reached horizontal acceleration peaks [7]. These seismic monitoring stations installed in the near-field area recorded a large amount of seismic wave data consisting of strong vertical ground shaking, which in

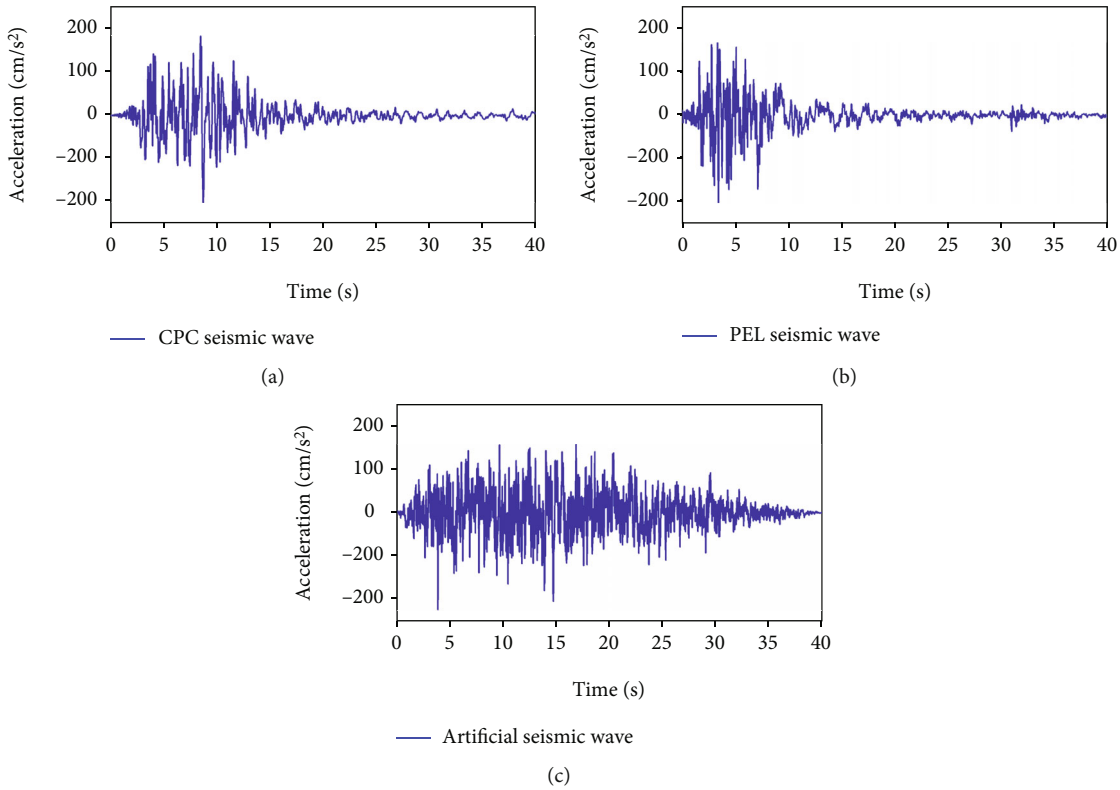

Figure 3: Time history acceleration diagram of different seismic waves.

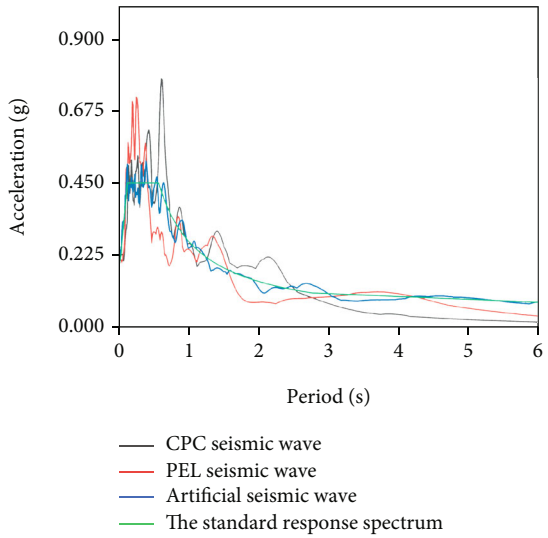

Figure 4: Acceleration response spectra of different seismic waves.

some places even exceeded the horizontal component of the earthquake [8]. The above phenomenon on vertical ground shaking attracts the attention of global scholars. Kamarroudi et al. [9] studied the effect of seismic vertical excitation on the P-Δ effect due to sway in an elevated water tank. The results showed that the sway height increased by about 20% due to the seismic vertical excitation and the P-Δ effect was amplified due to the sway and the inertial force caused by the vertical excitation. Shahbazi et al. [10] studied the seismic performance of special steel moment frames of 3-, 5-, 8-, and 20-story buildings under the vertical components of far-field and near-field earthquakes. It was shown that the forced displacements of the structure under the near-field earthquake were greater than those under the far-field earthquake. Fayaz and Zareian [11] assessed the effects of the vertical component of ground shaking on steel structures. Eight special moment-resisting frames (SMRF) and special concentric braced frame (SCBF) steel structures were analyzed, and the current seismic design provisions of ASCE 7 were evaluated in light of the structural reliability outlook. It was concluded that the seismic load combinations in ASCE 7 were inadequate to account for the effects of the vertical component of near-fault earthquakes; however, performance-based design provisions could provide reasonable and adequate safety margins for structural member failure. Wang et al. [12] used OPENSEES finite element software to carry out a nonlinear seismic analysis of power plant structures with extreme mass and stiffness irregularity and compared the impact of mass and stiffness irregularity on the risk of earthquake. Test results showed that vertical irregularities produced greater adverse effects than mass irregularities and required more attention in structural design; the greatest increase in collapse risk is due to the combined effects of mass and vertical irregularities. Liu et al. [13] analyzed the coupled horizontal and vertical rocking response of vertical isolated structures under near-fault seismic effects. It was found that the vertical isolated structure performed better in reducing the rocking response of the structure and vertical damping could significantly control the vertical displacement and rocking moment with increasing vertical period and

Table 1: Comparison table of base shear values.

Time history curve		Time history analysis		Mode response spectrum analysis		Ratios	
		X-direction (kN)	*Y*-direction (kN)	*X*-direction (kN)	*Y*-direction (kN)	*X*-direction (%)	*Y*-direction (%)
Model *a*	CPC	35933	27981	40128	32474	89.55%	86.16%
	PEL	34417	26018	40128	32474	85.77%	80.12%
	REN	40534	32674	40128	32474	101.01%	100.62%
	Average	36961	28891	40128	32474	92.11%	88.97%
Model *b*	CPC	46860	38297	45969	37284	101.94%	102.72%
	PEL	34240	28678	45969	37284	74.49%	76.92%
	REN	32966	26555	45969	37284	71.71%	71.22%
	Average	38022	31177	45969	37284	82.71%	83.62%
Model *c*	CPC	31643	28916	31915	31265	99.15%	92.49%
	PEL	34925	25952	31915	31265	110.37%	89.75%
	REN	32247	28687	31915	31265	92.33%	110.54%
	Average	32938	27852	31915	31265	102.14%	97.09%

Table 2: The parameters of the isolated bearing.

Structural model	Nonseismically isolated structures			Isolated structure	
	Maximum column bottom reaction force (kN)	Allowable compressive stress (MPa)	Minimum calculated diameter (mm)	Actual selection of the use of diameter (mm)	Actual compressive stress (MPa)
Model *a*	6410.12	12	824.91	1000	8.12
Model *b*	6387.21	12	823.44	1000	8.08
Model *c*	6353.30	12	821.25	1000	8.02

Table 3: Vibration period of different staggered structures.

Order of vibration	Model *a*		Model *b*		Model *c*	
	Nonisolated (s)	Isolated (s)	Nonisolated (s)	Isolated (s)	Nonisolated (s)	Isolated (s)
1	1.091	2.439	0.715	2.256	0.441	0.500
2	1.054	2.350	0.685	2.023	0.431	0.490
3	1.006	2.171	0.652	1.777	0.399	0.454
4	0.342	0.661	0.258	0.669	0.349	0.431
5	0.330	0.617	0.254	0.660	0.324	0.403

damping ratio. Zhou et al. [14] proposed a new nonlinear vibration isolated system designed for buildings with vibration isolated in the vertical direction and examined their applicability. The above studies pay attention to the different response effects of vertical ground shaking in three-dimensional earthquakes on different research objects, the isolated methods, and measures. However, the above studies all take the basic isolation as the precondition. The bases of building structures are not always on the same level to adapt to mountainous terrain. Since the bases of mountain buildings are not on the same level, a staggered floor isolated structure is proposed that can adapt to the terrain and at the same time achieve isolation. The staggered floor isolated structure is developed to adapt to the terrain in the evolution of base isolation, for example, Haikou Meilan Airport [15], as shown in Figure 1.

At present, there are relatively few studies on the three-dimensional seismic response considering the vertical component of the earthquake in the staggered layer at different heights, and the theory lags behind the practical application. Therefore, three staggered floor isolated structures with different heights of the staggered floor are established, and a finite element dynamic time-history analysis method is used, the response of the structure and the influence of the height of the isolated layer on the seismic response are studied under one-dimensional, two-dimensional, and three-dimensional earthquakes.

2. Materials and Methods

2.1. Model Overview. According to Chinese standard GB50011-2010 [16], the finite element analysis software SAP2000 is used to establish three staggered floor frame structures, which are models *a*, *b*, and *c* with different

Table 4: Mass participation coefficients of the first three orders of vibration.

Structural model	Model *a*			Model *b*			Model *c*		
Order of vibration	1	2	3	1	2	3	1	2	3
UX	0.00	0.98	0.00	0.00	0.98	0.00	0.23	0.00	0.00
UY	0.73	0.00	0.25	0.63	0.00	0.35	0.00	0.38	0.00
UZ	0.00	0.00	0.00	0.00	0.00	0.00	0.00	0.00	0.00
SumUX	0.00	0.98	0.98	0.00	0.98	0.98	0.23	0.23	0.23
SumUY	0.73	0.73	0.98	0.63	0.63	0.98	0.00	0.38	0.38
SumUZ	0.00	0.00	0.00	0.00	0.00	0.00	0.00	0.00	0.00
RX	0.00	0.00	0.01	0.00	0.00	0.03	0.00	0.07	0.05
RY	0.00	0.00	0.00	0.00	0.00	0.00	0.09	0.00	0.00
RZ	0.24	0.00	0.74	0.35	0.00	0.64	0.00	0.25	0.03
SumRX	0.00	0.00	0.01	0.00	0.00	0.04	0.00	0.07	0.12
SumRY	0.00	0.00	0.00	0.00	0.00	0.00	0.09	0.09	0.09
SumRZ	0.24	0.24	0.98	0.35	0.35	0.98	0.00	0.25	0.29

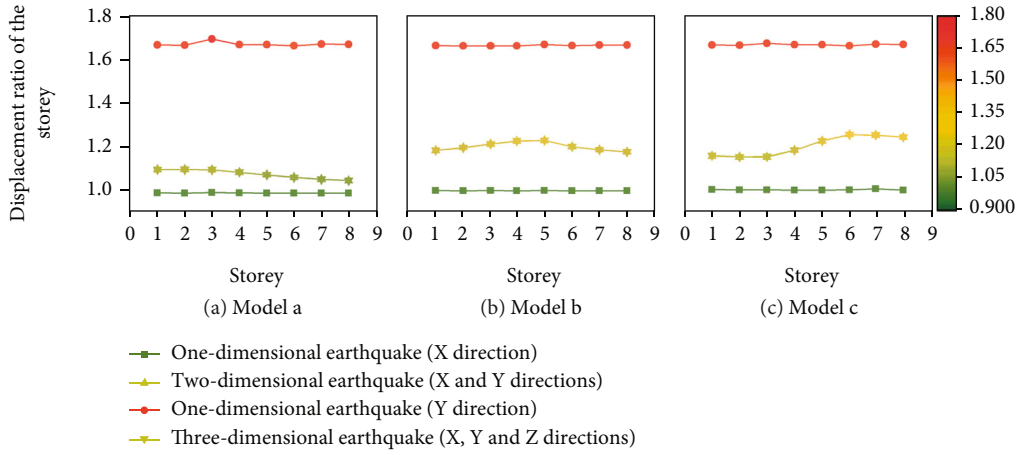

Figure 5: Floor displacement ratio in *X*-direction of different models under different dimensional earthquakes.

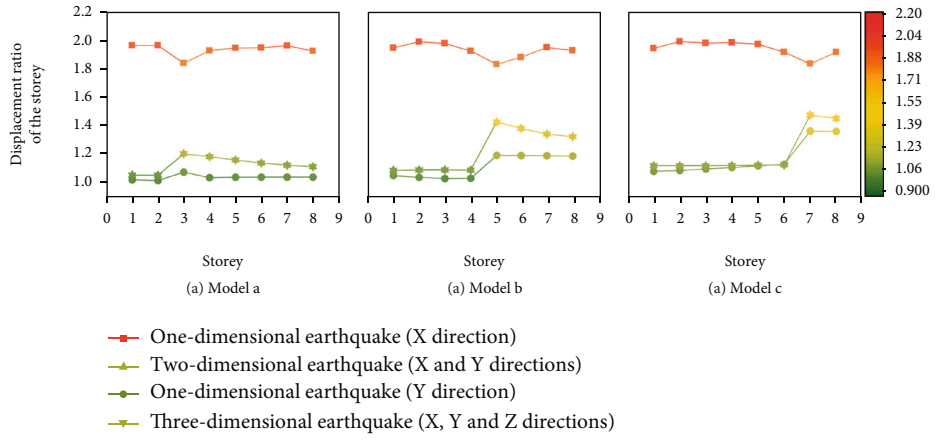

Figure 6: Floor displacement ratio in *Y*-direction of different models under different dimensional earthquakes.

staggered floor heights. There are 8 spans in *X*-direction and 5 spans in *Y*-direction. The spans are both 6 m in *X* - and *Y*-directions, and the floor height is 3.6 m. The staggered floors of models *a*, *b*, and *c* are 2, 4, and 6 floors, respectively. The isolated layer includes the upper isolated layer and the lower isolated layer. The live load of the floor is 2 kN/m^2, and the dead load is 3 kN/m^2. The thickness of the upper floor of the isolated layer is 180 mm, and that of the other floors is 120 mm. The column section is 700 mm × 700 mm, and the beam section is 700 mm × 300

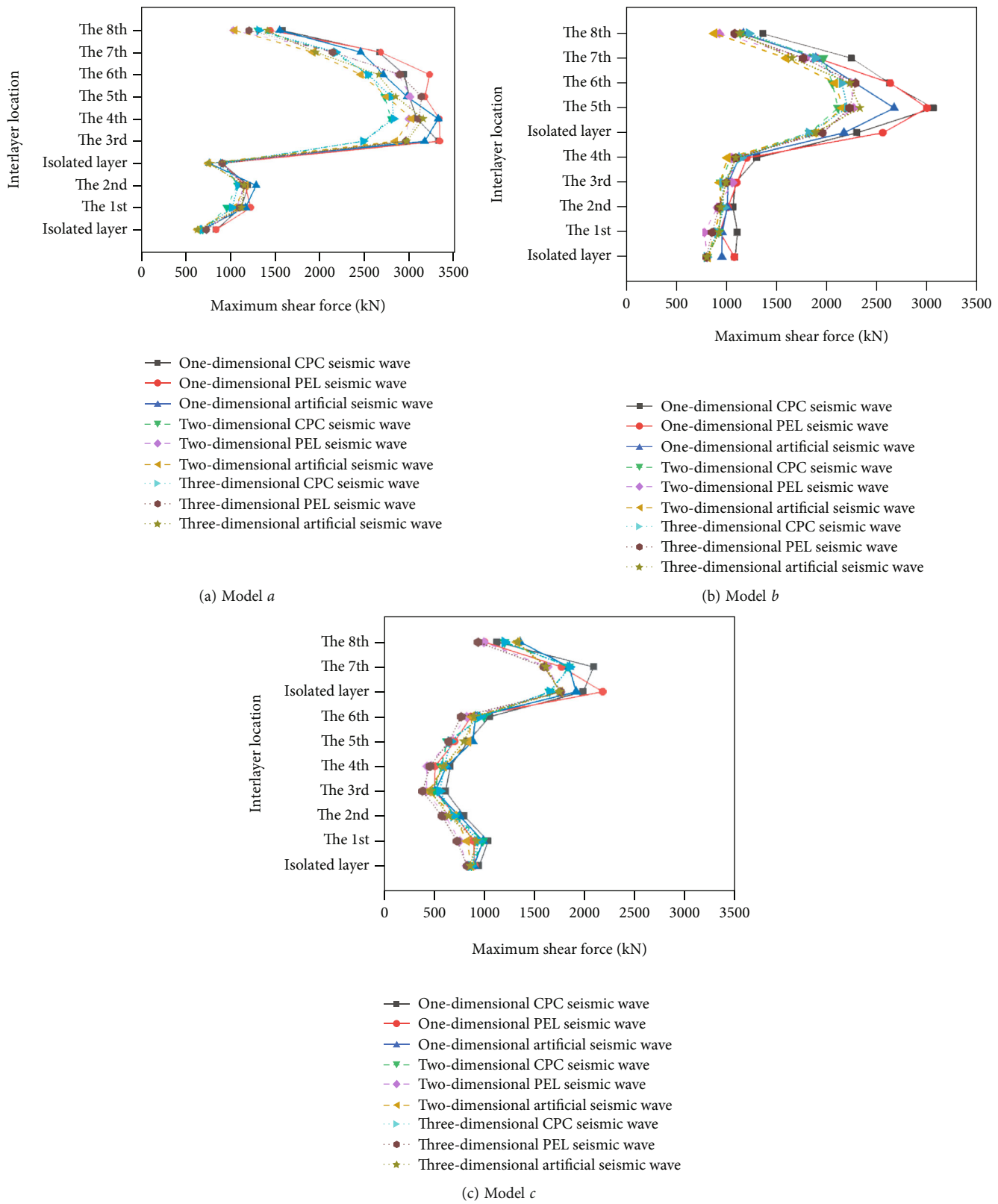

Figure 7: Comparison of interlayer shear force in X-direction of different models.

mm. The concrete strength grade is C30, the longitudinal stressed reinforcement is HRB400, and the stirrup is HPB300. The height of the isolated layer is 1.6 m. The isolated bearing is simulated by damping units in SAP2000. The structural model and reinforcement diagram of the isolated frame are shown in Figure 2.

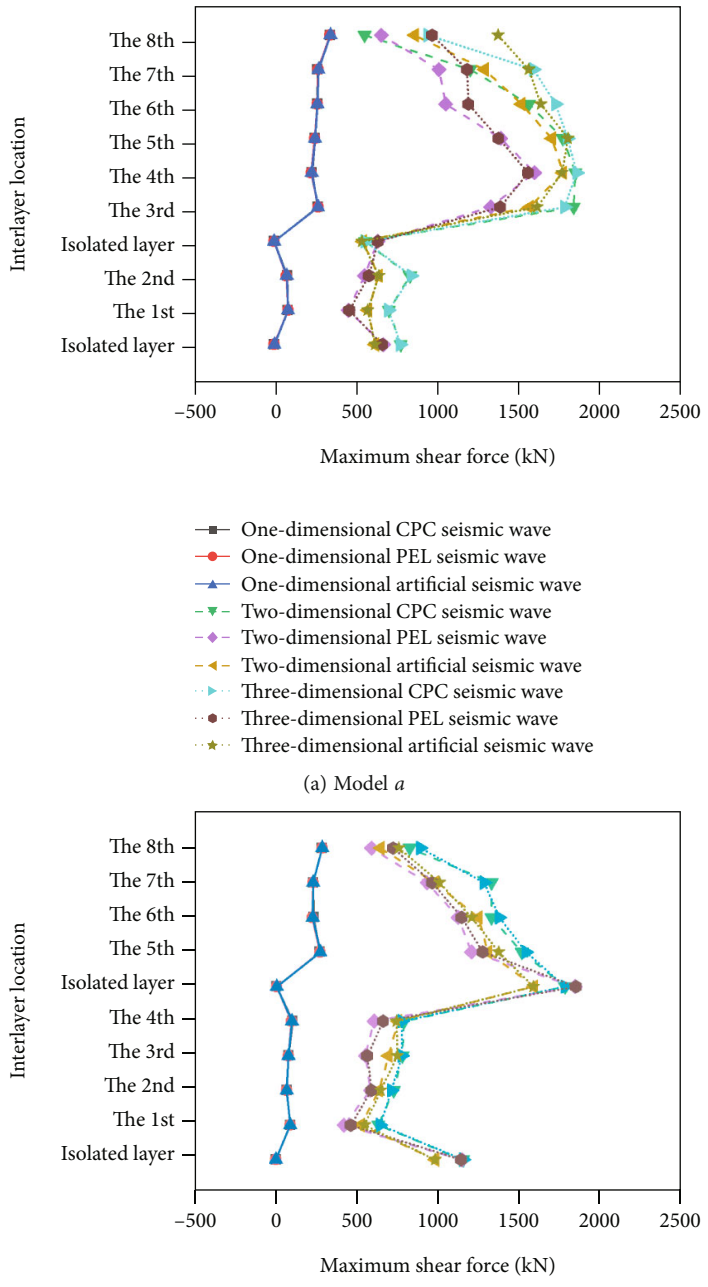

(a) Model *a*

(b) Model *b*

Figure 8: Continued.

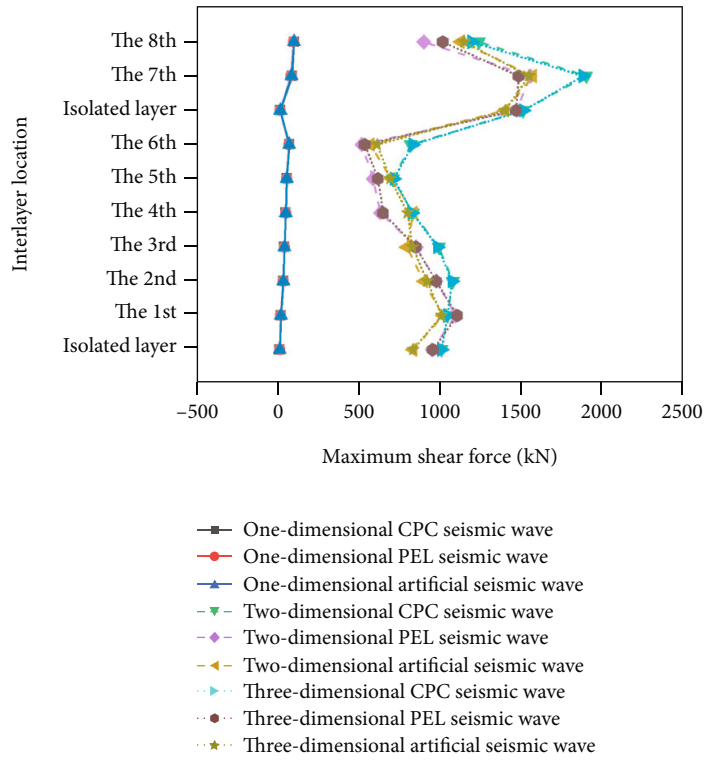

(c) Model *c*

Figure 8: Comparison of interlayer shear force in *Y*-direction of different models.

2.2. Selection and Checking Calculation of Seismic Waves. According to Chinese standards GB50011-2021 [17] and GB/T51408-2021 [18], the seismic intensity of the project is 8 degrees. The maximum seismic acceleration is 200 cm/s^2, the site soil category is class III, the design seismic grouping is group II, and the characteristic period of the site is Tg = 0.55 s. The actual seismic wave CPC wave with a sampling interval of 0.02 s and a peak acceleration of 348.07 cm/s^2 and the actual seismic wave PEL wave with a sampling interval of 0.02 s and a peak acceleration of 174.17 cm/s^2 are both from the Pacific Geoengineering Research Center (PEER) ground motion database. The seismic wave with a sampling interval of 0.01 s and a peak acceleration of 157.65 cm/s^2 of artificially simulated seismic wave was generated based on the response spectrum method [19]. The amplitudes of all three seismic waves were adjusted to the seismic fortification intensity level [20]. The three seismic wave curves and response spectra are shown in Figures 3 and 4.

The structural basal shear calculated by each seismic wave should exceed 65% of the results of the spectrum method, and the average value of all seismic waves should exceed 80% of the results of the spectrum method [17]. The comparison of the basal shear values is shown in Table 1. According to the results in the table, all three seismic waves meet the requirements.

2.3. Selection of Isolated Bearing. The isolated bearing selection is carried out for the established models *a*, *b*, and *c*. LRB1000 isolated bearing is selected, the thickness of the rubber is 162 mm, the vertical stiffness is 6878 kN/m, the 100% equivalent horizontal stiffness is 4238 kN/m, the 100% equivalent damping ratio is 0.23, the preyield stiffness is 20626 kN/m, the postyield stiffness is 2623 kN/m, and the yield force is 261.7 kN. According to Chinese standard GB50011-2021 [17], the vertical compressive stress of the rubber isolated bearing shall not exceed 12 MPa under the representative value of gravity load. The actual maximum surface pressure of the isolated bearing of model *a* is 8.12 MPa, the isolated bearing of model *b* is 8.08 MPa, and the isolated bearing of model *c* is 8.02 MPa, which all meet the requirements of the above specifications. The specific parameters of the isolated bearing are shown in Table 2.

3. Analysis and Results

3.1. Analysis of Dynamic Characteristics of Staggered Floor Isolated Structures. The vibration period of the isolated structure of models *a*, *b*, and *c* is effectively extended compared with the nonisolated structure as shown in Table 3. The vibration period of model *a* is larger than that of model *b*, and the period of model *b* is larger than that of model *c*.

3.2. Torsional Analysis of Staggered Floor Isolated Structures under Three-Dimensional Earthquakes. The ratio of the seismic waves' peak acceleration input to the staggered floor isolated structures was 1 : 0.85 : 0.65 [21], and the dynamic response of the structures in different directions were analyzed and compared by inputting seismic waves from *X*-direction alone, *Y*-direction alone, and *X*-direction and *Y*-direction

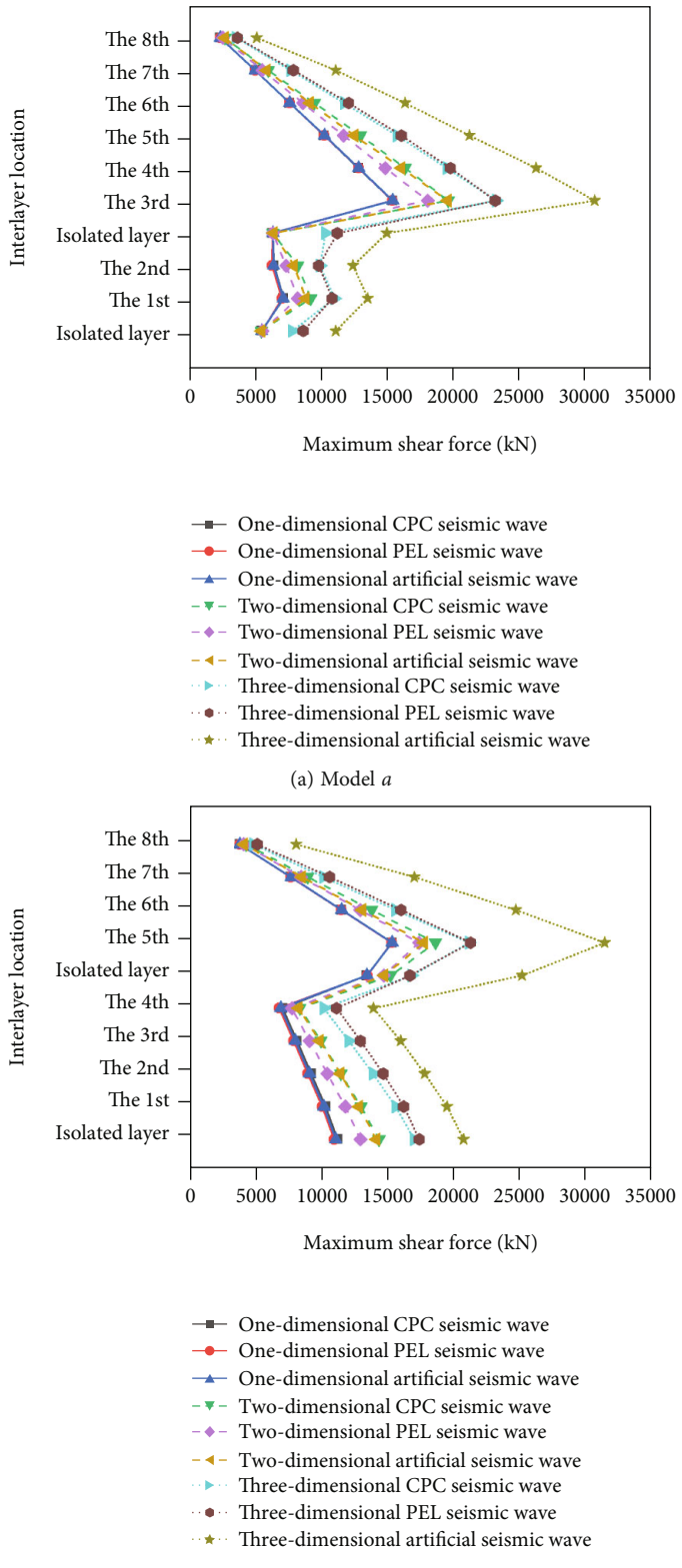

(a) Model *a*

(b) Model *b*

Figure 9: Continued.

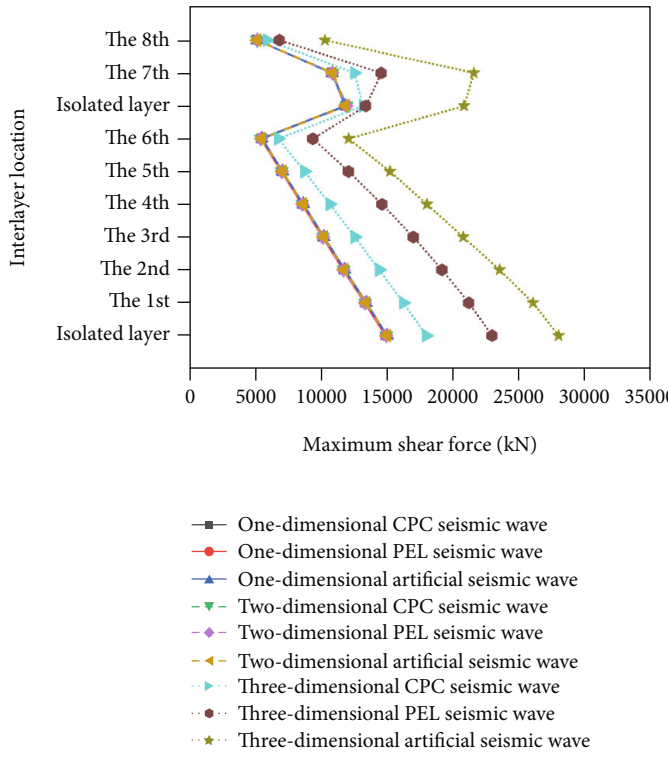

(c) Model *c*

Figure 9: Comparison of the maximum axial force between different models.

together and from *X*-direction, *Y*-direction, and Z-direction together. The staggered floor isolated structure is an asymmetric structure with the center of mass deviating from the center of stiffness, which makes the structure undergo horizontal vibration and torsional vibration at the same time [22–24].

3.2.1. Analysis of the Torsional Period Ratio. The torsional period ratio is the ratio of the first vibration period dominated by torsion to the first vibration period dominated by horizontal movement. It is necessary to control the torsional period ratio to make sure that the structure has sufficient torsional stiffness [25].

The results show that the first vibration period of model *a* is 2.17 s for structural torsion and 2.44 s for structural horizontal movement, with a period ratio of 0.89; the first vibration period of model *b* is 1.78 s for structural torsion and 2.26 s for structural horizontal movement, with a period ratio of 0.78; the first vibration period of model *c* is 0.45 s for structural torsion and 0.5 s for structural horizontal movement, with a period ratio of 0.9. As the height of the staggered floors changes, the center of mass and the center of stiffness also change. The vibrational mass participation coefficients of models *a*, *b*, and *c* are shown in Table 4.

3.2.2. Analysis of the Floor Displacement Ratio. The floor displacement ratio is the ratio of the maximum and the average value of the elastic horizontal displacement (interstory displacement). The smaller the floor displacement ratio, the smaller the torsional effect of the structure. The purpose of controlling the displacement ratio is to limit the torsion of the structure [26]. Take the actual seismic wave CPC wave as an example; the floor displacements of the structure in *X*-direction and *Y*-direction under CPC seismic wave in different dimensions are shown in Figures 5 and 6.

It can be seen from Figures 5 and 6 that (1) the input of seismic waves in the *X*-direction has no obvious effect on the floor displacement ratio of the structure in the *X*-direction since the staggered isolated models are symmetrical in the *X*-direction. Compared with the input of seismic wave in *X*-direction alone, the floor displacement ratio in the *X*-direction of the structure has an increasing effect under the joint input of seismic wave *X*-direction and *Y*-direction. (2) The addition of seismic wave in *Z*-direction contributes less to the floor displacement ratio.

3.3. Analysis of Interlayer Shear Forces under Three-Dimensional Earthquakes

3.3.1. Analysis of Interlayer Shear Force in X-Direction. The results of interlayer shear force of staggered floor isolated structure under three-dimensional earthquake are shown in Figures 7 and 8. As shown in Figure 7, (1) the maximum interlayer shear force in the *X*-direction is mainly concentrated in the staggered layer. (2) The three-dimensional earthquakes contribute less to the interlayer shear in the *X*-direction of the structure compared with the two-dimensional earthquakes.

3.3.2. Analysis of Interlayer Shear Force in Y-Direction. As shown in Figure 8, (1) the input of seismic wave in the *X*-direction has little effect on the interlayer shear force in

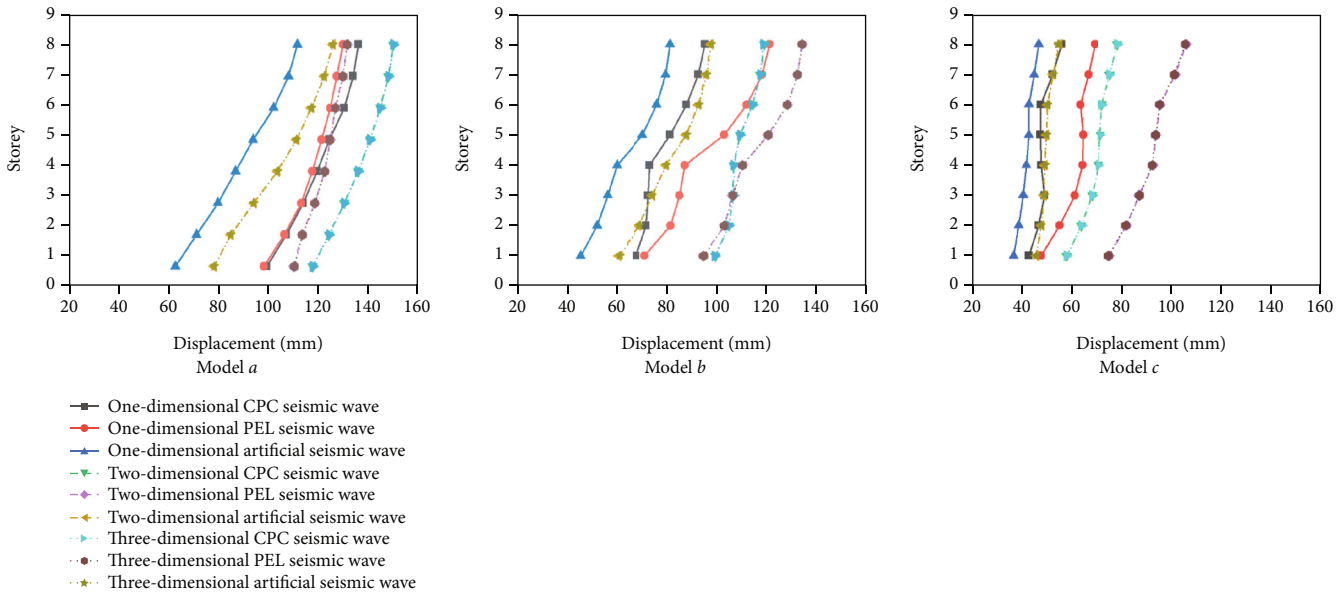

Figure 10: Comparison of floor displacements of different models in X-direction.

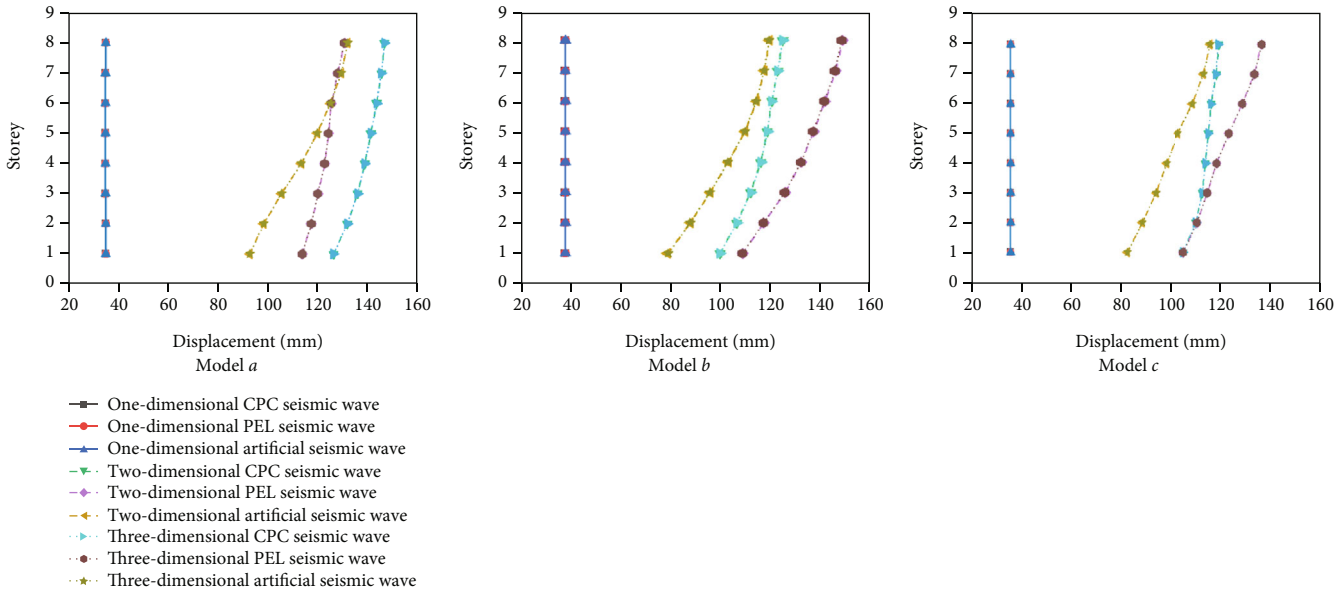

Figure 11: Comparison of floor displacements of different models in Y-direction.

the Y-direction of the structure, while the input of seismic wave in the Y-direction has a great contribution to the interlayer shear force in Y-direction of the structure, and the maximum interlayer shear force in Y-direction of the structure is mainly concentrated in the staggered layers. (2) Compared with two-dimensional horizontal earthquakes, the addition of earthquakes in Z-direction has less contribution to the maximum value of interlayer shear force.

3.4. Analysis of the Maximum Axial Force under Three-Dimensional Earthquakes. The results of the maximum axial force in the staggered floor isolated structures under three-dimensional earthquakes are shown in Figure 9. As shown in Figure 9, (1) the maximum axial force decreases with the increase in floor height; however, (2) the input of three-dimensional earthquake in Z-direction can enhance the vertical maximum axial force of the isolated layer. (3) Compared with one-dimensional X-direction earthquake, the input of two-dimensional X-direction and Y-direction earthquake and input of three-dimensional earthquake in X-, Y-, and Z-directions tend to increase the maximum axial force.

3.5. Analysis of the Floor Displacement under Three-Dimensional Earthquakes

3.5.1. Analysis of Floor Displacement in X-Direction. The floor displacement results of staggered floor isolated

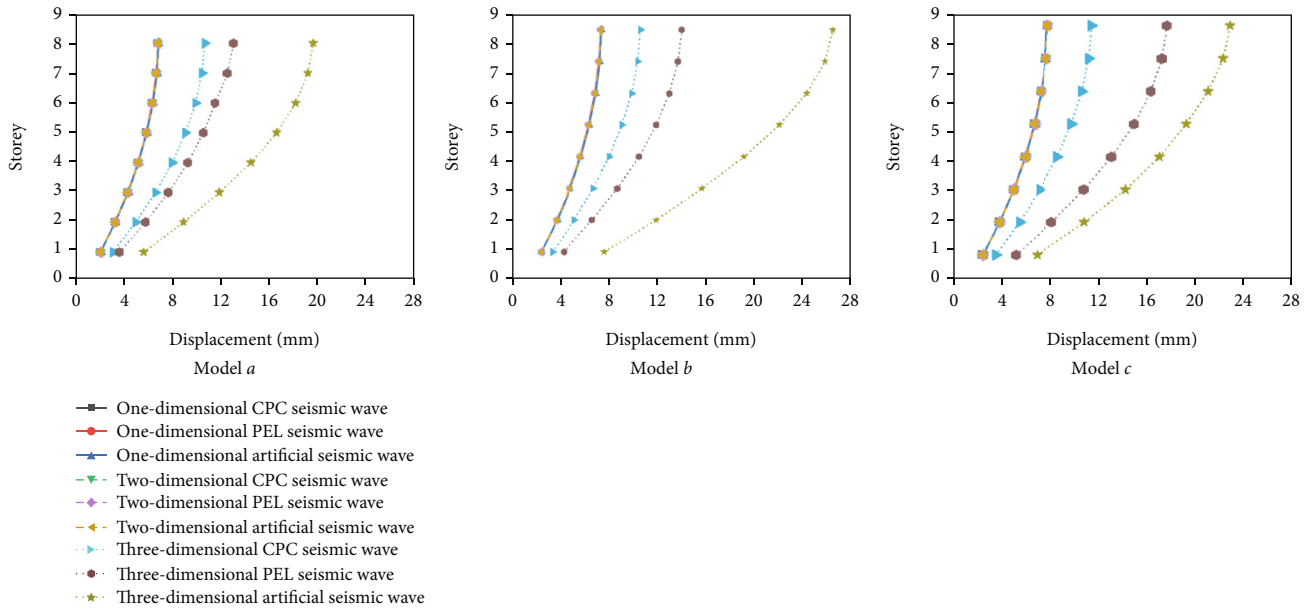

Figure 12: Comparison of floor displacements of different models in Z-direction.

structures under three-dimensional earthquakes are shown in Figures 10–12. It can be seen from Figure 10 that (1) the displacement of floors in the X-direction of the structure increases with the increase in floor height. (2) The addition of Z-direction of three-dimensional earthquakes has little contribution to the horizontal displacement of the floor.

3.5.2. Analysis of Floor Displacement in Y-Direction. It can be seen from Figure 11 that (1) the input in the X-direction of one-dimensional earthquake has little effect on the floor displacement in the Y-direction of the structure. (2) The input in the Y-direction of one-dimensional earthquake plays a major role in the floor displacement of the Y-direction of the structure. (3) The three-dimensional seismic waves in Z-direction have little contribution to the horizontal displacement of the structure.

3.5.3. Analysis of Floor Displacement in Z-Direction. It can be seen from Figure 12 that (1) the floor displacement of the structure in the Z-direction increases with the increase in floor height. (2) The two-dimensional earthquakes have little contribution to the floor displacement of the structure in the vertical Z-direction. (3) The three-dimensional seismic waves of Z-direction greatly increase the floor displacement of the structure in the Z-direction.

3.6. Results of Staggered Isolated Structures. The results in this paper are consistent with the results of the multidimensional seismic response shaker test study [27]. The horizontal dynamic response of the base-isolated model is weakened. Due to the horizontal-vertical coupling effect, the response under three-dimensional earthquake input is larger than that under one-dimensional and two-dimensional input [28]. However, the most interesting and surprising thing about this study is that the isolated layer is not on the same horizontal plane, resulting in the noncoincidence of the stiffness center and mass center of the structure, which makes the structure move not only horizontally but also torsionally.

4. Discussion

In this paper, we found that the staggered floor isolated structure has the advantages of base isolated structure at the same time [29, 30]. The practical project Haikou Meilan Airport [15] shows that the staggered isolated structures have a good isolated effect. This paper establishes three staggered floor isolated frames with different staggered floor heights. At the same time, we know that our study has some limitations and the response of the actual staggered isolated structure is very complex under earthquakes. There are many factors that should be considered, such as landslide deformation [31], failure characteristics of sandstone under different envelope pressures [32], the influence of seismic force on slope stability [33], the influence of seismic activity during geological mining [34], and the difference between hard rock and soft rock [35, 36].

5. Conclusion

In this paper, through the establishment of three different heights of the staggered isolated structure in mountainous areas, the dynamic characteristics, structural torsion, interstory shear force, maximum axial force, and response of floor displacement of the staggered isolated structure are compared by numerical simulations under different seismic waves inputs, which complement the theoretical study of staggered isolated structures; the main conclusions are listed as follows:

(1) In the case of one-dimensional earthquake, the staggered isolated structure belongs to the asymmetric

structure and the stiffness center deviates from the center of mass; both horizontal vibration and torsional vibration occur in the structure

(2) In the case of two-dimensional earthquakes, the interstory shear force, the maximum axial force, the floor displacement, and the floor displacement ratio increase in varying degrees compared with those in one-dimensional earthquake input

(3) In the case of three-dimensional earthquakes, the vertical seismic wave has a great contribution to the maximum axial force; however, the influence of the vertical seismic wave on the shear force, horizontal displacement, and torsion effect is less obvious

(4) The location between the upper isolated layer and the first floor above the upper isolated layer is the weak part of the staggered isolated structure

Data Availability

All data included in this study are available upon request by contact with the corresponding author.

Conflicts of Interest

The authors declare that there is no conflict of interest regarding the publication of this paper.

References

[1] S. Cheng, D. Liu, S. Fang et al., "Study on the impact of hydraulic fracturing on surrounding ancillary buildings considering SSI," *Geofluids*, vol. 2021, Article ID 1850705, 12 pages, 2021.

[2] T. Chen, Z. Wu, Y. Mu, P. Wang, and Q. Zhu, "Numerical analysis of seismic site effects in loess region of western China under strong earthquake excitations," *Shock and Vibration*, vol. 2020, Article ID 3918352, 12 pages, 2020.

[3] C. X. Nie, Q. S. Chen, G. Y. Gao, and J. Yang, "Determination of seismic compression of sand subjected to two horizontal components of earthquake ground motions," *Soil Dynamics and Earthquake Engineering*, vol. 92, pp. 330–333, 2017.

[4] S. Hashemi and M. H. Aghashiri, "Seismic responses of base-isolated flexible rectangular fluid containers under horizontal ground motion," *Soil Dynamics and Earthquake Engineering*, vol. 100, pp. 159–168, 2017.

[5] Y. Zhou, C. Wu, C. Zhang, and G. Yang, "Analysis and design of seismic isolation structure of the outpatient complex of Lushan County People's Hospital," *Building Structure*, vol. 24, pp. 23–27, 2013.

[6] W. Suzuki, S. Aoi, and H. Sekiguchi, "Rupture process of the 2008 Iwate-Miyagi Nairiku, Japan, earthquake derived from near-source strong-motion records," *Bulletin of the Seismological Society of America*, vol. 100, no. 1, pp. 256–266, 2010.

[7] Z. Wang, "A preliminary report on the great Wenchuan earthquake," *Earthquake Engineering and Engineering Vibration*, vol. 7, no. 2, pp. 225–234, 2008.

[8] C. C. Harrington and A. B. Liel, "Collapse assessment of moment frame buildings, considering vertical ground shaking," *Earthquake Engineering & Structural Dynamics*, vol. 45, no. 15, pp. 2475–2493, 2016.

[9] S. H. Kamarroudi, M. Hosseini, and K. Hosseini, "Influence of earthquake vertical excitations on sloshing-created P-Δ effect in elevated water tanks: experimental validation, numerical simulation and proposing a modification for Housner model," *Engineering Structures*, vol. 246, article 112995, 2021.

[10] S. Shahbazi, I. Mansouri, J. W. Hu, N. S. Daliri, and A. Karami, "Seismic response of steel SMFs subjected to vertical components of far-and near-field earthquakes with forwarding directivity effects," *Advances in Civil Engineering*, vol. 2019, Article ID 2647387, 15 pages, 2019.

[11] J. Fayaz and F. Zareian, "Reliability analysis of steel SMRF and SCBF structures considering the vertical component of near-fault ground motions," *Journal of Structural Engineering*, vol. 145, no. 7, 2019.

[12] J. Wang, K. Dai, Y. Yin, and S. Tesfamariam, "Seismic performance-based design and risk analysis of thermal power plant building with consideration of vertical and mass irregularities," *Engineering Structures*, vol. 164, pp. 141–154, 2018.

[13] D. Liu, Y. Zhang, S. Fang, and Y. Liu, "Horizontal-vertical-rocking coupled response analysis of vertical seismic isolated structure under near-fault earthquakes," *Shock and Vibration*, vol. 2020, Article ID 6519808, 10 pages, 2020.

[14] Y. Zhou, P. Chen, and G. Mosqueda, "Analytical and numerical investigation of quasi-zero stiffness vertical isolation system," *Journal of Engineering Mechanics*, vol. 145, no. 6, 2019.

[15] H. Liang, S. Guo, L. Wang, F. Wang, H. Zheng, and H. Tan, "Construction technology of split-level seismic isolation for the second-phase terminal of Meilan Airport," *Engineering Construction and Design*, vol. 424, no. 2, pp. 150–152, 2020.

[16] National Standard of the People's Republic of China (NSPRC), *Chinese Code for Design of Concrete Structures (GB50011-2010)*, Ministry of Housing and Urban-Rural Development of the People's Republic of China, Beijing, China, 2015, (in Chinese).

[17] National Standard of the People's Republic of China (NSPRC), *Chinese Code for Seismic Design of Buildings (GB50011-2021)*, Ministry of Housing and Urban-Rural Development of the People's Republic of China, Beijing, China, 2021, (in Chinese).

[18] National Standard of the People's Republic of China (NSPRC), *Chinese Standard for Seismic Isolation Design of Building (GB/T 51408-2021)*, Ministry of Housing and Urban-Rural Development of the People's Republic of China, Beijing, China, 2021, (in Chinese).

[19] B. Wei, L. Yan, L. Jiang, Z. Hu, and S. Li, "Errors of structural seismic responses caused by frequency filtering based on seismic wave synthesis," *Soil Dynamics and Earthquake Engineering*, vol. 149, article 106862, 2021.

[20] L. Pei and Y. Wenjian, "Comparative study of seismic wave selection methods in Sino-US seismic design," *Structural Engineer*, vol. 29, no. 6, pp. 7–13, 2013, (in Chinese).

[21] Y. Li, C. Bu, K. Liu, H. Zhou, and F. Zhu, "Shaking table test of simple energy dissipation masonry structure model," *Journal of Chongqing University*, vol. 36, no. 6, pp. 46–52, 2013, (in Chinese).

[22] M. A. Hussain and S. C. Dutta, "Inelastic seismic behavior of asymmetric structures under bidirectional ground motion: an effort to incorporate the effect of bidirectional interaction in load resisting elements," *Structure*, vol. 25, pp. 241–255, 2020.

[23] O. Akyurek, *Lateral and Torsional Seismic Vibration Control for Torsionally Irregular Buildings*, no. article 27721124,

2019Florida Institute of Technology ProQuest Dissertations Publishing, 2019.

[24] C. G. Karayannis and M. C. Naoum, "Torsional behavior of multistory RC frame structures due to asymmetric seismic interaction," *Engineering Structures*, vol. 163, pp. 93–111, 2018.

[25] R. Hoult and K. Beyer, "Decay of torsional stiffness in RC U-shaped walls," *Journal of Structural Engineering*, vol. 146, no. 9, 2020.

[26] B. Khanal and H. Chaulagain, "Seismic elastic performance of L-shaped building frames through plan irregularities," *Structure*, vol. 27, pp. 22–36, 2020.

[27] W. Xu, D. Du, S. Wang, W. Liu, and W. Li, "Shaking table tests on the multi-dimensional seismic response of long-span grid structure with base-isolation," *Engineering Structures*, vol. 201, 2019.

[28] J. Zhao, D. Liu, S. Yao et al., "Study on response of mid-storey isolation structure with SSI effect subjected to three-dimensional ground motions," *Journal of Seismological Research*, vol. 44, no. 4, pp. 665–672, 2021, (in Chinese).

[29] H. Jun, L. Yingmin, and T. Gelin, "Influence of ground support types on the seismic performance of structures supported by foundations at different ground levels," *China Civil Engineering Journal*, vol. 47, Suppl 2, pp. 93–100, 2014.

[30] L. P. Wang, H. P. Zhong, and L. Q. Huang, "Analysis on seismic behavior of structures supported by foundations with different locations," *Advanced Materials Research*, vol. 690-693, pp. 824–828, 2013.

[31] X. Chen, D. Li, X. Tang, and Y. Liu, "A three-dimensional large-deformation random finite-element study of landslide runout considering spatially varying soil," *Landslides*, vol. 18, no. 9, p. 3249, 2021.

[32] Z. Liu, H. Zhou, W. Zhang, S. Xie, and J. Shao, "A new experimental method for tensile property study of quartz sandstone under confining pressure," *International Journal of Rock Mechanics and Mining Sciences*, vol. 123, 2019.

[33] W. Zhang, F. Meng, F. Chen, and H. L. Liu, "Effects of spatial variability of weak layer and seismic randomness on rock slope stability and reliability analysis," *Soil Dynamics and Earthquake Engineering*, vol. 146, 2021.

[34] F. De Santis, V. Renaud, Y. Gunzburger, J. Kinscher, P. Bernard, and I. Contrucci, "In situ monitoring and 3D geomechanical numerical modelling to evaluate seismic and aseismic rock deformation in response to deep mining," *International Journal of Rock Mechanics and Mining Sciences*, vol. 129, article 104273, 2020.

[35] Z. Wang and Q. Liu, "Failure criterion for soft rocks considering intermediate principal stress," *International Journal of Mining Science and Technology*, vol. 31, no. 4, pp. 565–575, 2021.

[36] G. Han, Y. Zhou, R. Liu, Q. Tang, X. Wang, and L. Song, "Influence of surface roughness on shear behaviors of rock joints under constant normal load and stiffness boundary conditions," *Natural Hazards*, vol. 112, no. 1, pp. 367–385, 2022.